ISSN 1990-7931, Russian Journal of Physical Chemistry B, 2020, Vol. 14, No. 2, pp. 362–366. © Pleiades Publishing, Ltd., 2020.
Russian Text © The Author(s), 2020, published in Khimicheskaya Fizika, 2020, Vol. 39, No. 4, pp. 63–67.

CHEMICAL PHYSICS
OF ATMOSPHERIC PHENOMENA

Simulation of Ionospheric Effects Induced by Meteorological Storms

I. V. Karpov[a, b, *], O. P. Borchevkina[a, b], and P. A. Vasilev[a, b]

[a] *Immanuel Kant Baltic Federal University, Kaliningrad, 236041 Russia*
[b] *Kaliningrad Branch of Pushkov Institute of Terrestrial Magnetism, Ionosphere, and Radio Wave Propagation, Russian Academy of Sciences, Kaliningrad, 236010 Russia*
**e-mail: ivkarpov@inbox.ru*

Received February 20, 2019; revised May 14, 2019; accepted May 20, 2019

Abstract—The paper presents the results of a numerical simulation of ionospheric disturbances caused by a point thermospheric heat source, which mimic the dissipation effect of acoustic-gravity waves propagating from the region of a meteorological storm. It is shown that ionospheric effects have an extensive spatial structure and are more pronounced during the day than at night. The results of numerical simulations show decreases in the critical frequency of the F2 layer (*fo*F2) and in the total concentration of electrons to the northwest from the heat source maximum, as well as increases in the values of these parameters to the south and southeast from the heat source maximum up to the equatorial region. A comparative analysis of the daytime and nighttime disturbances of atmospheric parameters is given, and a conclusion is drawn on the causes of weakly pronounced changes in the nighttime ionosphere.

Keywords: ionosphere, acoustic-gravity waves, thermosphere, numerical experiment
DOI: 10.1134/S1990793120020220

INTRODUCTION

As has been established in experimental studies, active dynamic processes in the lower atmosphere, such as typhoons, hurricanes, and storms, cause a variety of ionospheric disturbances [1–5]. Thus, significant decreases in the total electron content (TEC) have been detected above the regions of meteorological disturbances when observing the dynamics of the ionosphere during periods of meteorological disturbances [6]. In particular, decreases in the daytime TEC values reaching about 50% relative to meteorologically calm days have been noted in numerous observations made in the Kaliningrad region during the periods of sharp worsening of weather conditions, which are accompanied by escalation of squally winds up to force 8–9 on the Beaufort scale [7]. The peculiarities of the observed ionospheric disturbances consist in the fact that they appear above the storm area and are strongly correlated in time with the increased wind gust speeds in the storm region [6, 7].

As proposed in [6, 8], such ionospheric disturbances may be caused by dissipation of acoustic-gravity waves (AGWs) which are excited in the region of a meteorological disturbance and propagate into the upper atmosphere. It can be assumed that the squally nature of the wind during periods of meteorological disturbances reflects the processes of enhancement of AGW generation. Theoretical studies show that infrasonic waves and AGWs with periods close to the Väisälä–Brunt period can reach the altitudes of the thermosphere and ionosphere when propagating almost vertically from the excitation region [9–11]. The dissipation of such waves leads to the formation of local heat regions in the thermosphere [11, 12], which can affect the dynamics of the ionosphere and ionization–recombination processes.

The aim of this study was to simulate the reaction of the upper atmosphere and ionosphere to the appearance of a local thermal perturbation in the thermosphere, which mimics the effects of the dissipation of waves that propagate from the region of the meteorological disturbance.

PROBLEM STATEMENT AND DESCRIPTION OF THE NUMERICAL EXPERIMENTAL

To estimate the spatial structure and amplitude of the source of thermosphere perturbation due to dissipation of AGWs, the calculations performed for the published theoretical study [13] were used. A was shown in [13], the propagation of infrasound waves and AGWs from the Earth's surface with periods close to the Väisälä–Brunt period leads to the formation of a heated region above the source of disturbance at altitudes of about 200 km due to the dissipation of waves. Setting the amplitudes of wave disturbances to values that are typical for weather storms at the Earth's surface gives rise to heating of the thermosphere by about 100 K in such processes.

To investigate the effect of the additional thermospheric heat source on the parameters of the upper atmosphere and ionosphere, numerical experiments with use of the global self-consistent model of the thermosphere, ionosphere, and protonosphere (GSM TIP) were carried out [14]. The GSM TIP model allows one to calculate global distributions of thermospheric and ionospheric parameters within the altitude range of 80 to 500 km and has been successfully used to study large-scale processes in the upper atmosphere [15–17].

To simulate the influence of a source that mimics the effect of the dissipation of AGWs on the thermosphere and ionosphere condition, we include additional heat source Q, defined by expression

$$Q\ [\mathrm{K/min}] = A\exp\left(-\frac{|r-r_0|}{H}\right), \quad (1)$$

where r is the altitude, $r_0 = 180$ km is the altitude of the heat source maximum, and H is the altitude of the homogeneous atmosphere, in the thermal balance equation of the ionosphere in the GSM TIP model at a location with a specified latitude and longitude. Altitude r_0 in Eq. (1) was determined using a qualitative interpretation of the results by simulating the dissipation of AGWs from a ground-level source [13]. Amplitude factor A was chosen so that the maximum heating of the thermosphere at an altitude of r_0 was 100 K, and the A value in this study was 20 K/min. In addition, the GSM TIP equations consider that the density perturbation caused by such large-scale heating can be taken into account by the following polarization relations published in [18]:

$$\frac{\Delta T_d}{T} = -\frac{\Delta\rho_d}{\rho}, \quad (2)$$

where ΔT_d and $\Delta\rho_d$ are the temperature and density increments, respectively; T and ρ are the background values of the temperature and density, respectively.

Numerical calculations were performed to simulate the daily dynamics of an unperturbed atmosphere and the effect of an additional heat source, which mimic the influence of AGW dissipation on the upper atmosphere. The source was placed in the location with coordinates at 45° N and 15° E. The initial conditions were specified in such a way that the state of the atmosphere corresponded to the end of December.

RESULTS AND DISCUSSION

The simulation covered a daily interval beginning at midnight UT. Two types of numerical experiments, namely, experiments with a nighttime heat source that turns on at midnight and an experiment with a daytime source that turns on at 10 UT, were performed. The source continued to operate in both cases until the end of the day. In both cases, the reaction of the ionosphere parameters was detected an hour after the source was turned on and reached a maximum of 16 UT.

Figure 1 shows the latitudinal–longitudinal distributions of the *fo*F2 disturbances. The results of calculation show that perturbations of the critical frequency are small when the additional source is turned on at midnight (Fig. 1a), and their spatial structure is quite complex, covering a significant part of the northern hemisphere. A decrease in the *fo*F2 value is observed right above the source, whereas this parameter, on the contrary, increases in the equatorial region and has an increment with a periodic structure. Over the entire nighttime period, the values of the increment to *fo*F2 barely exceed 0.1 MHz and have no substantial effect on the state of the ionosphere.

In the daytime (Fig. 1b), an enhanced effect of the source is observed both at the equator, where the increment reaches 0.15 MHz, and in the region with a clearly pronounced maximum with an increment value of about 0.4 MHz to the south of the source location. A region with a critical frequency decreased by about 0.1–0.15 MHz, which is elongated by 20° to the west, is detected to the northwest of the heat source maximum. It should be noted that the spatial structure of the critical frequency perturbation for a daytime source that began operation at 10 UT, is similar to the structure of perturbations caused by the operation of the nighttime source (Fig. 1c).

Figure 2 shows the spatial perturbations of TEC. At nighttime (Fig. 2a), there is a pronounced maximum to the southeast of the source. Although the mid-latitude TEC perturbations have small absolute values, their relative deviations from the background value significantly exceed those for *fo*F2. Namely, the deviations reach 8% in TEC and are about 1.5% in *fo*F2.

The structure of the TEC perturbations in the daytime (Figs. 2b and 2c) generally repeats the structure of the *fo*F2 perturbations for both the nighttime and daytime sources. It should be noted that a local maximum and a local minimum zonal symmetrical to it appear at low latitudes of the northern hemisphere and in the southern hemisphere, respectively. This is revealed in the calculation results for the nighttime source (Fig. 2b).

In both *fo*F2 and TEC, the small difference between the daytime ionospheric effects for the nighttime and daytime sources is worthy of note. Figure 3 shows the vertical profiles of the increments to the dynamic parameters of the atmosphere at the point of a maximum negative effect of *fo*F2, which is shifted by 5° N and 5° W from the point of maximum thermospheric heating.

Despite the fact that a substantial increase in the temperature and changes in the O/N_2 ratio and velocity components are observed just a few hours after the start of the calculation of the nighttime source (Figs. 3b–3f), this does not cause substantial fluctuations in the *fo*F2

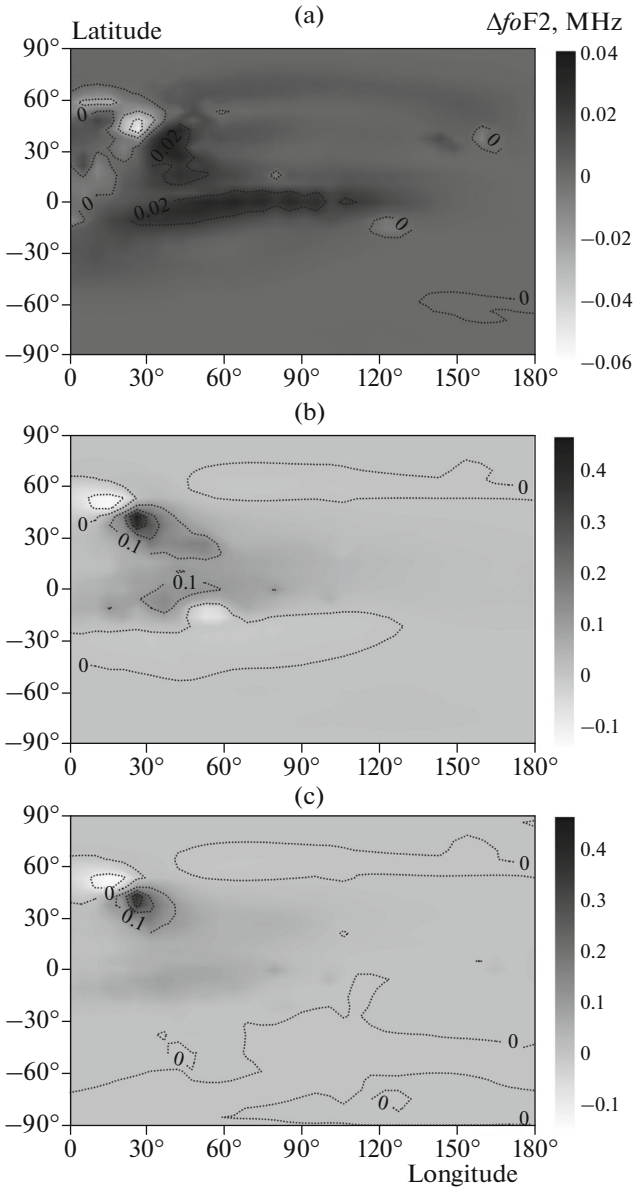

Fig. 1. Distribution of the increment to *fo*F2 in MHz at (a) 6 and (b) 16 UT for a nighttime source and (c) 16 UT for a daytime source.

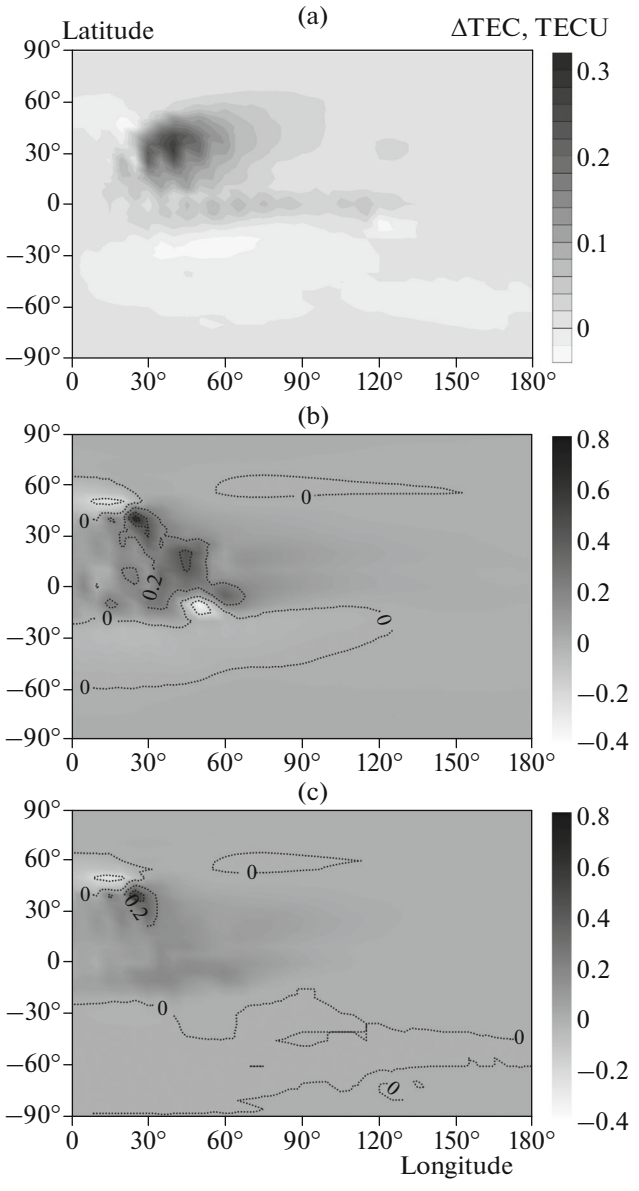

Fig. 2. Distribution of the increment to TEC (measured in TECU) at (a) 6 and (b) 16 UT for a nighttime source and (c) 16 UT for a daytime source.

value (Fig. 3a). At the same time, the dynamics of deviations of all key parameters are close in both cases starting from 12 UT and give rise to similar effects with respect to *fo*F2.

In addition, some parameters, such as temperature increments (Fig. 3c), ratios of concentration of atomic oxygen to molecular nitrogen (Fig. 3b), and meridional velocity (Fig. 3e), are reduced by the end of the calculation. This behavior may be caused by the fact that an additional thermosphere heat source has an insignificant effect on the ionosphere at night and, consequently, critical frequency perturbations in both calculation versions present a similar spatial structure to perturbations.

Nearly the same dynamics of changes in the thermosphere parameters in both calculation versions for the daytime are associated, apparently, with strong localization of the source of perturbations. In this regard, substantial thermospheric disturbances arise near the source region and the dynamics of thermosphere changes in the region of the maximum negative disturbance of the ionosphere (northwest of the thermospheric source) are similar in both cases of operation of the nighttime and daytime sources.

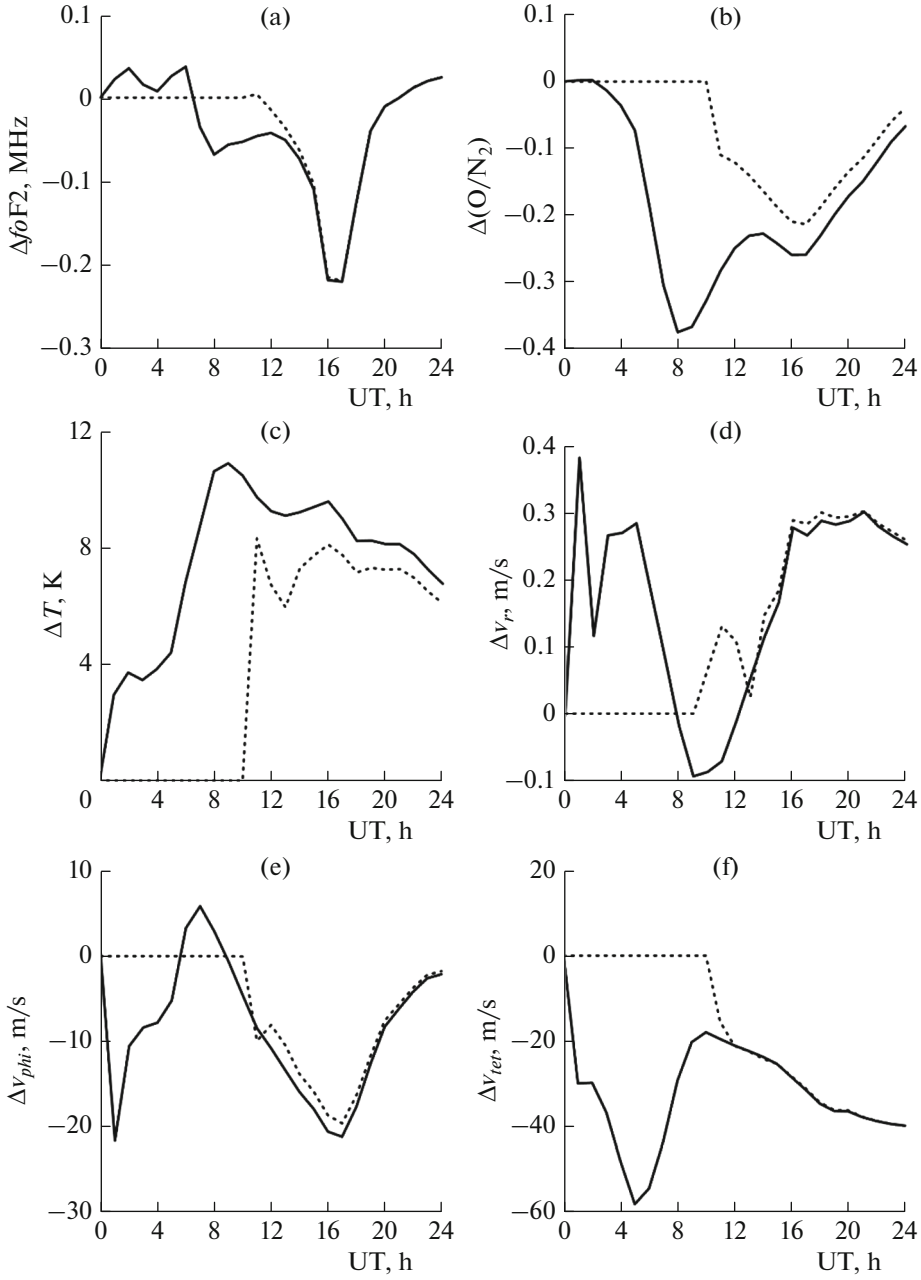

Fig. 3. The dependences of the increments to (a) *fo*F2, (b) to the concentration ratio of atomic oxygen to molecular nitrogen, to (c) the temperature, and to the (d) vertical (v_τ), (e) meridional (v_{phi}), and (f) zonal (v_{tet}) velocities for calculations performed with a source that operated starting from 0 UT (solid line) and 10 UT (dashed line) at the altitude of the heat source maximum, i.e., 180 km, in the region of maximum negative ionospheric effects to the northwest from the source.

CONCLUSIONS

The simulation of ionospheric effects induced by thermospheric heating caused by dissipation of AGWs reveals a decrease in the electron concentration at the F-layer maximum of the daytime ionosphere to the northwest from the source region and an increase in the electron concentration to the south and southeast from the source region. The generated perturbations quickly spread over large distances and reach the equatorial region.

The nighttime ionospheric effects of the thermosphere disturbances are substantially weaker than the daytime ones, despite comparable disturbances in the main dynamic parameters. This may be because local perturbations of the thermosphere at night have a weak effect on the ionosphere.

Experimental studies show that ionospheric disturbances induced by storms significantly exceed the disturbances revealed in the calculation results. Thus, the experimentally observed decreases in TEC can reach 50% relative to calm weather conditions. In numerical calculations, the decrease in this parameter did not exceed 10%. Presumably, the inclusion of only the temperature source of thermosphere disturbance caused by dissipation of AGWs does not give an adequate result and a more sophisticated description of the source of thermosphere disturbance with the inclusion of wind perturbations is required.

FUNDING

This study was supported by grant nos. 18-05-00184-a (I.V. Karpov) and 17-05-00574-a (O.P. Borchevkina) from the Russian Foundation for Basic Research, and grant no. 17-17-01060 (P.A. Vasilev) from the Russian Science Foundation.

REFERENCES

1. M. A. Chernigovskaya, B. G. Shpynev, and K. G. Ratovsky, J. Atmos. Sol.-Terr. Phys. **136**, 235 (2015). https://doi.org/10.1016/j.jastp.2015.07.006
2. W. Li, J. Yue, Y. Yang, et al., J. Atmos. Sol.-Terr. Phys. **161**, 43 (2017). https://doi.org/10.1016/j.jastp.2017.06.012
3. C. R. Martinis and J. R. Manzano, Ann. Geofis. **42** (1), 1 (1999).
4. E. Yigit, P. K. Knizova, K. Georgieva, et al., J. Atmos. Sol.-Terr. Phys. **141**, 1 (2016). https://doi.org/10.1016/j.jastp.2016.02.011
5. O. P. Suslova, I. V. Karpov, and A. V. Radievskii, Russ. J. Phys. Chem. B **7**, 652 (2013). https://doi.org/10.7868/S0207401X13090124
6. O. P. Borchevkina and I. V. Karpov, Geomagn. Aeron. **57**, 624 (2017). https://doi.org/10.7868/S0016794017040046
7. I. V. Karpov, O. P. Borchevkina, R. Z. Dadashev, et al., Soln.-Zemn. Fiz. **2** (2), 64 (2016). https://doi.org/10.12737/21001
8. I. V. Karpov, S. P. Kshevetskii, O. P. Borchevkina, A. V. Radievsky, and A. I. Karpov, Russ. J. Phys. Chem. B **10**, 127 (2016). https://doi.org/10.7868/S0207401X16010064
9. M. P. Hickey, R. L. Walterscheid, and G. Schubert, J. Geophys. Res. A **116**, 12326 (2011). https://doi.org/10.1029/2010JA016792
10. G. Schubert, M. P. Hickey, and R. L. Walterscheid, J. Geophys. Res. A **110**, D07106 (2005). https://doi.org/10.1029/2004JD005488
11. I. V. Karpov and S. P. Kshevetskii, Geomagn. Aeron. **54**, 513 (2014). https://doi.org/10.7868/S001679401404018X
12. S. L. Vadas and H. Liu, J. Geophys. Res. **114** (A10), 310 (2009). https://doi.org/10.1029/2009JA014108
13. I. V. Karpov and S. P. Kshevetskii, J. Atmos. Sol.-Terr. Phys. **164**, 89 (2017). https://doi.org/10.1016/j.jastp.2017.07.019
14. A. A. Namgaladze, Yu. N. Koren'kov, V. V. Klimenko, et al., Geomagn. Aeron. **30**, 612 (1990).
15. M. V. Klimenko, V. V. Klimenko, Yu. N. Koren'kov, F. S. Bessarab, I. V. Karpov, K. G. Ratovsky, and M. A. Chernigovskaya, Cosmic Res. **51**, 54 (2013). https://doi.org/10.7868/S0023420613010056
16. I. V. Karpov, F. S. Bessarab, Yu. N. Korenkov, V. V. Klimenko, and M. V. Klimenko, Russ. J. Phys. Chem. B **10**, 117 (2016). https://doi.org/10.7868/S0207401X16010052
17. I. V. Karpov, F. S. Bessarab, O. P. Borchevkina, K. A. Artemenko, and A. I. Klopova, Geomagn. Aeron. **58**, 509 (2018). https://doi.org/10.1134/S0016794018040089
18. G. I. Grigor'ev, Izv. Vyssh. Uchebn. Zaved., Radiofiz. **42** (1), 3 (1999).

Translated by O. Kadkin